Supporting Information

Controlling Synthesis of Uniform Electron Deficient Pd Clusters for Superior Hydrogen Production from Formic Acid

Wanyue Ye,[a,#] Wei Pei,[b,#] Si Zhou,[b] He Huang,[a] Qian Li,[a] Jijun Zhao,[b] Rongwen Lu,*[,a] Yuzhen Ge*[,c] and Shufen Zhang[a]

[a]State Key Laboratory of Fine Chemicals, Dalian University of Technology, Dalian 116024, China

[b]Education Ministry Key Lab of Materials Modification by Laser, Ion and Electron Beams, Dalian University of Technology, Dalian 116024, China

[c]College of Chemistry and Molecular Engineering, Peking University, Beijing 100871, China

Corresponding Author
Rongwen Lu, email: lurw@dlut.edu.cn
Yuzhen Ge, email: gyzhen822@pku.edu.cn

[#]Wanyue Ye and Wei Pei contributed equally to this work.

1. Experimental Data

Chemicals

Polyoxyethylene (20) cetyl ether (Brij®58, Acros Organics), ammonium hydroxide ($NH_3 \cdot H_2O$, 25%−28%, Tianjin Damao Chemical Reagent Co. Inc., China), tetraethyl orthosilicate (TEOS, Sinopharm Chemical Reagent Co., Ltd.), (3-aminopropyl)-triethoxysilane (APTES, Shanghai Aladdin Biochemical Polytron Technologies Inc.), cyclohexane (Sinopharm Chemical Reagent Co., Ltd.), isopropanol (IPA, Sinopharm Chemical Reagent Co., Ltd.), ammonium tetrachloropalladate (II) ($(NH_4)_2PdCl_4$, Sinopharm Chemical Reagent Co., Ltd.), *p*-phenylenediamine (Beijing J&K Scientific Ltd., China), trisodium citrate dihydrate ($C_6H_5Na_3O_7 \cdot 2H_2O$, Na_3Cit, Tianjin Damao Chemical Reagent Co. Inc., China), potassium permanganate ($KMnO_4$, Tianjin Guangfu Fine Chemical Research Institute), graphite (Tianjin Bodi Chemical Co., Ltd.), concentrated phosphoric acid (Tianjin Fuyu Fine Chemical Co., Ltd.), concentrated sulfuric acid (H_2SO_4, 98%, Tianjin Chemical Reagent Factory), hydrochloric acid (HCl, Tianjin Chemical Reagent Factory), sodium borohydride ($NaBH_4$, Sinopharm Chemical Reagent Co., Ltd.), formic acid (FA, 98%, Shanghai Aladdin Biochemical Technology Co., Ltd.).

Characterization

TEM images were captured by a Tecnai G^2 20 S-Twin transmission electron microscopy (TEM) at an accelerating voltage of 300 kV. Scanning transmission electron microscopy (STEM) and energy-dispersive X-ray spectroscopic (EDS) data were recorded with a JEM-2100F instrument operating at 200 kV. The XRD patterns were recorded on a Rigaku DMAX IIIVC X-ray diffractometer with Cu Ka (0.1542 nm) radiation scanning from 5° to 90° (2θ) at the rate of $5° \cdot min^{-1}$. X-ray photoelectron spectroscopy (XPS) was acquired by ThermoFisher ESCALAB™ 250 Xi with an Al Kα X-ray source operating at 150 W (15 kV). The binding energies were calibrated

using the C 1s peak at 284.6 eV, and the software XPS PEAK 4.1 was used for curve fitting. Raman spectra were measured on a confocal laser micro-Raman spectrometer (Thermo DXR Microscope, USA). The content of Pd in all catalysts was determined by the inductively coupled plasma optical emission spectroscopy (ICP-OES, Optima 2000 DV, Perkin Elmer, US).

Synthesis of Pd/PDA-LGO

For testifying the necessity of silica support, we also prepared PDA functionalized large area GO (LGO) supported Pd nanoparticles (Pd/PDA-LGO). Typically, 60 mg of LGO were dispersed with 60 mL of water in a single-neck round-bottom flask to form a homogeneous solution. Subsequently, 9 mL of PDA acetone solution (480 mg PDA, 0.22 M) was added dropwise into the LGO suspension and stirring for 24 h. Then $(NH_4)_2PdCl_4$ aqueous solution (25 mL, 2.26 mM) were added dropwise into the above mixture with continuous stirring at 4 °C. The aqueous solution (1 mL, 0.17 M) and freshly prepared $NaBH_4$ aqueous solution (25 mL, 0.054 M) were injected directly into the above solution. After 30 min of reduction, the mixture was separated via centrifugation at 9000 rpm for 10 min and washed with water for two times. The products were dried at 100 °C for 5 h.

2. Computational methods

First-principles calculations were performed by density functional theory (DFT) calculations implemented in the Vienna Ab Initio Simulation Package (VASP) using the planewave basis set with an energy cutoff of 500 eV.[1] We used the projector augmented wave (PAW) pseudopotentials and the generalized gradient approximation parameterized by Perdew, Burke, and Ernzerhof (GGA-PBE) for exchange-correlation functional.[2-3] A three-layer slab model was adopted for the (111) surface of Pd metal with a 4 × 4 supercell for the lateral dimension. Graphene oxide is modelled by a supercell consisting of 5 × 5 graphene unit cells, with a pseudo-random distribution

of O and OH species having an O/C ratio of 0.2. The Brillouin zone of the supercell was sampled by a 3 × 3 × 1 Monkhorst-Pack **k** point mesh. With fixed lattice constant, the model structures were fully optimized by ionic and electronic degrees of freedom using the convergence criteria of 10^{-4} eV for electronic energy and 10^{-2} eV/ Å for the forces on each atom. The bottom layer of Pd(111) surface was fixed during geometrical optimization. Grimme's semiempirical DFT-D3 scheme of dispersion correction was used to describe the van der Waals (vdW) interactions.[4] The kinetic barriers and transition states for critical steps of FA dehydrogenation were simulated by the climbing-image nudged elastic band (CI-NEB) method implemented in VASP[5], using five images to mimic the reaction path. The intermediate images were relaxed until the perpendicular forces were less than 10^{-2} eV/ Å. On the basis of the equilibrium configurations from the VASP calculations, Mulliken charge analysis was employed by CASTEP code using the planewave basis with an energy cutoff of 1000 eV, norm-conserving pseudopotentials, and GGA-PBE functional.[6-7]

The FA decomposition process is considered to involve the following elemental steps:[8]

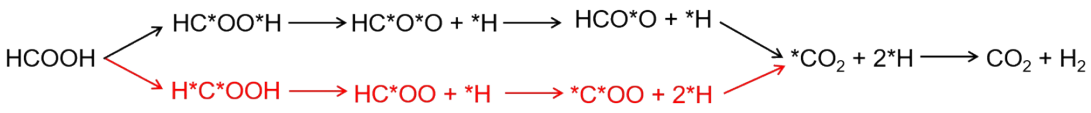

where black and red indicate the reaction pathway for Pd(111) and PDA-GO@Pd_8, respectively. *(X) indicates the adsorbed sites on the surface of systems. To characterize the interaction between catalyst and the adsorbate involved in FA dehydrogenation reaction, the binding energy is defined as:

$$\Delta E = E_{\text{total}} - E_{\text{cata}} - E_{\text{mol}} \quad \textbf{(1)}$$

where E_{total}, E_{cata}, and E_{mol} represent the energies of the adsorbate/catalyst system, clean catalyst, and adsorbate in the gas phase, respectively. The Gibbs free energy of formation for each reaction step is calculated by

$$\Delta G = \Delta E + \Delta \mathrm{ZPE} - T\Delta S \quad \textbf{(2)}$$

where ΔE, ΔZPE and ΔS are the differences of DFT total energy, zero-point energy, and entropy between the initial and final states, respectively; T is temperature and set to be 300 K in our calculations. The values of ΔZPE and ΔS of gaseous molecules can be obtained from the NIST-JANAF thermodynamics table and by calculated the vibrational frequencies for the reaction intermediates, respectively (see Table S4 for details).

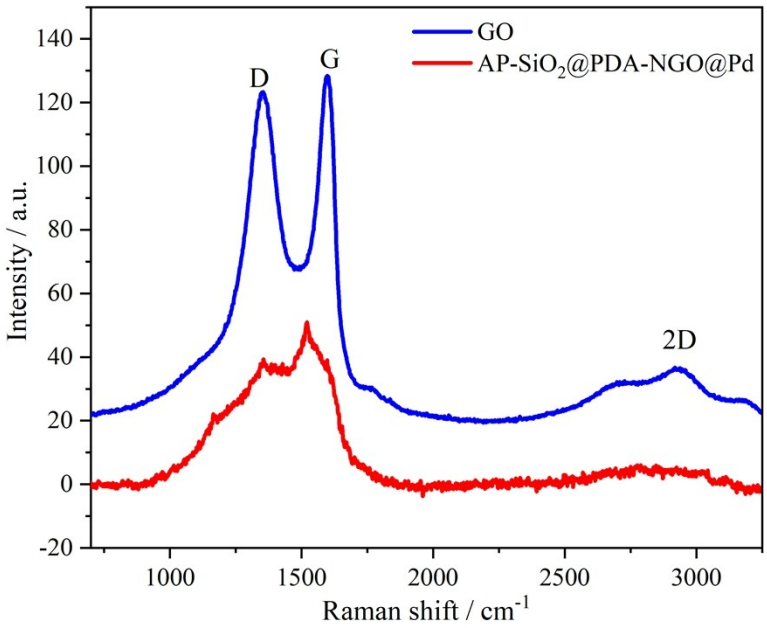

Figure S1 Raman spectra of GO and AP-SiO_2@PDA-NGO@Pd.

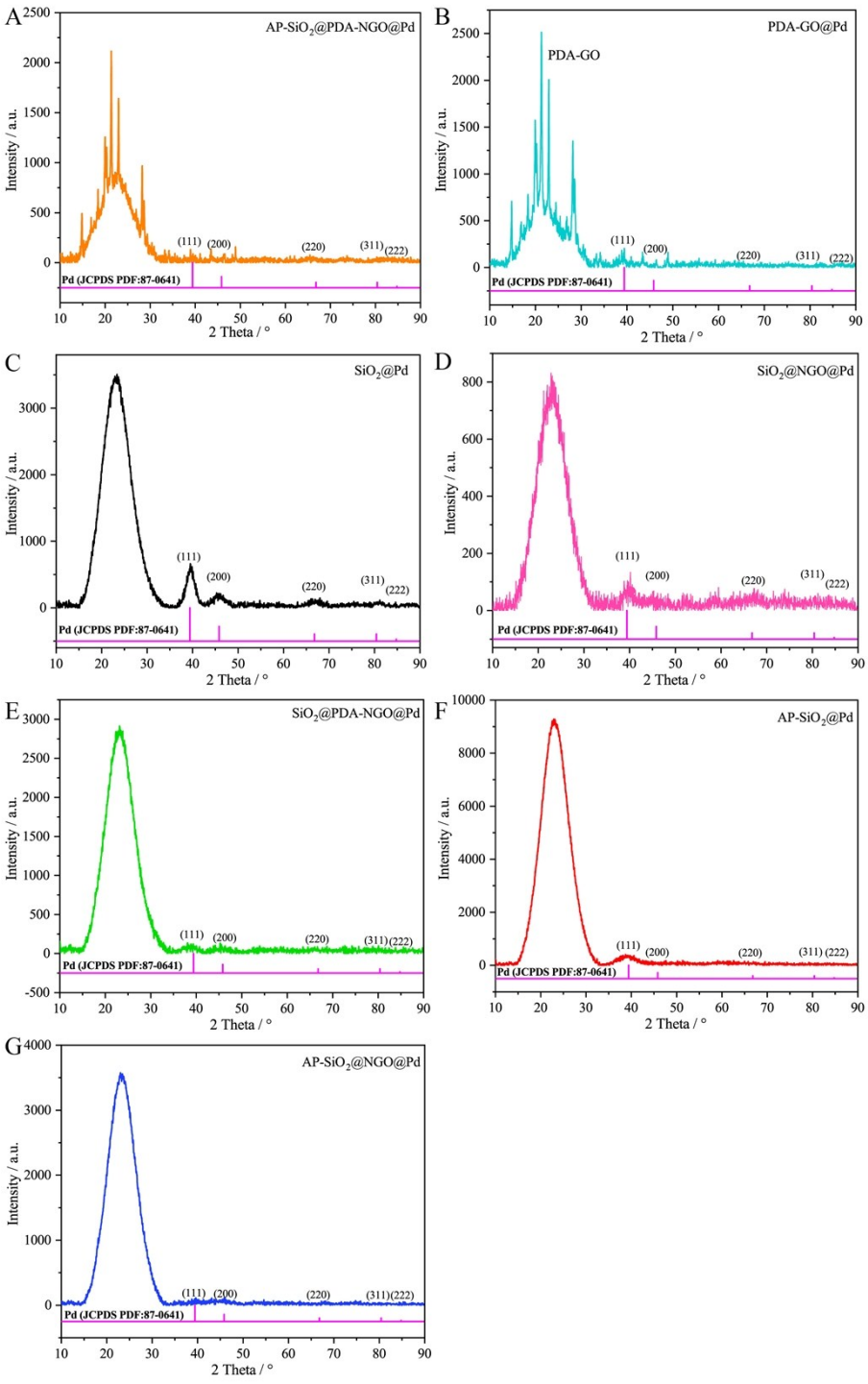

Figure S2 XRD patterns of Pd deposited on different structural supports: AP-SiO_2@PDA-NGO@Pd (A), PDA-GO@Pd (B), SiO_2@Pd (C), SiO_2@NGO@Pd (D), SiO_2@PDA-NGO@Pd (E), AP-SiO_2@Pd (F) and AP-SiO_2@NGO@Pd (G).

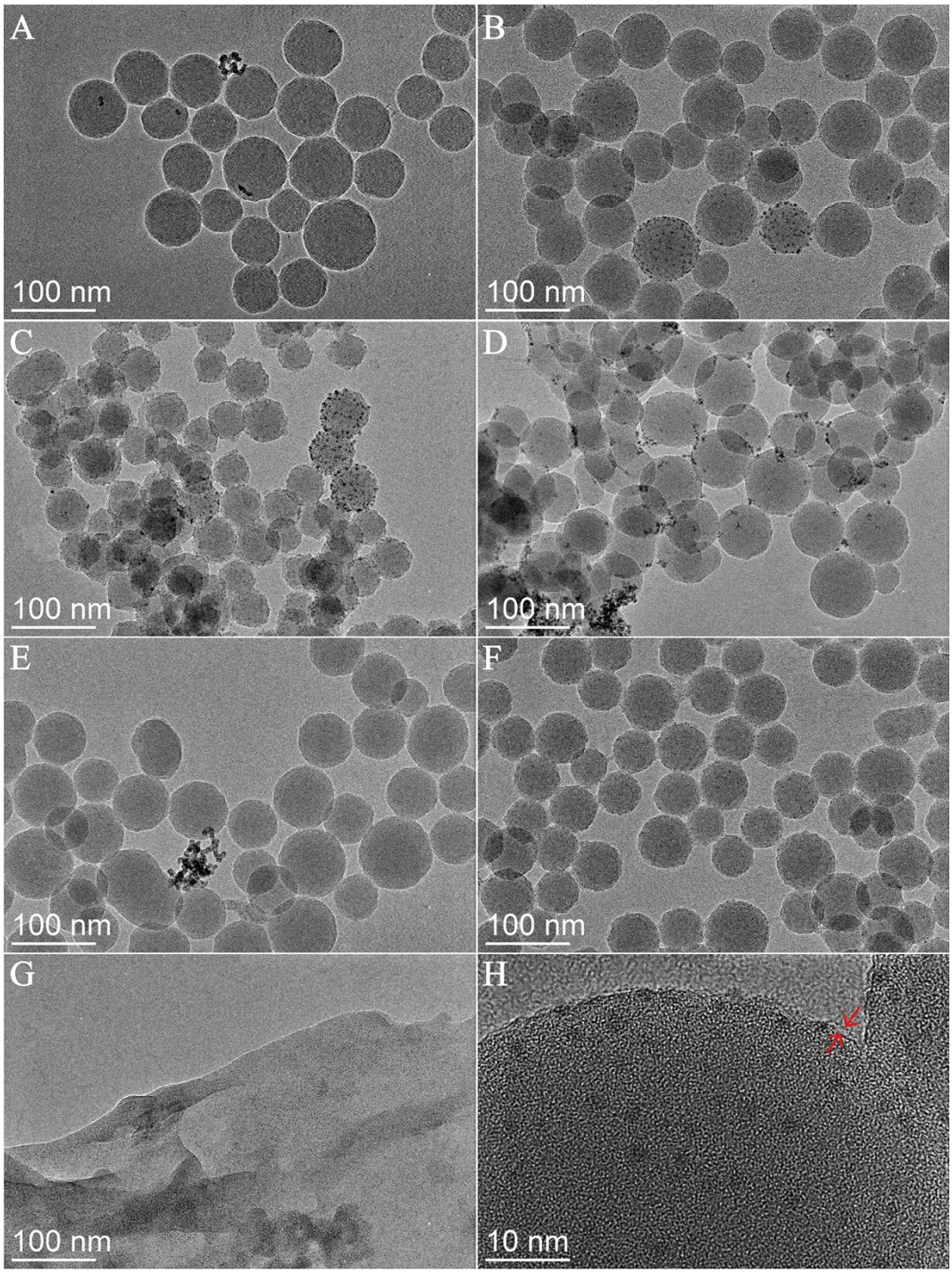

Figure S3 TEM images of SiO_2@Pd (A), AP-SiO_2@Pd (B), AP-SiO_2@NGO@Pd (C), SiO_2@PDA-NGO@Pd (D), SiO_2@NGO@Pd (E) and AP-SiO_2@PDA-NGO@Pd (F), PDA-GO@Pd (G) and HRTEM image of AP-SiO_2@PDA-NGO@Pd (H).

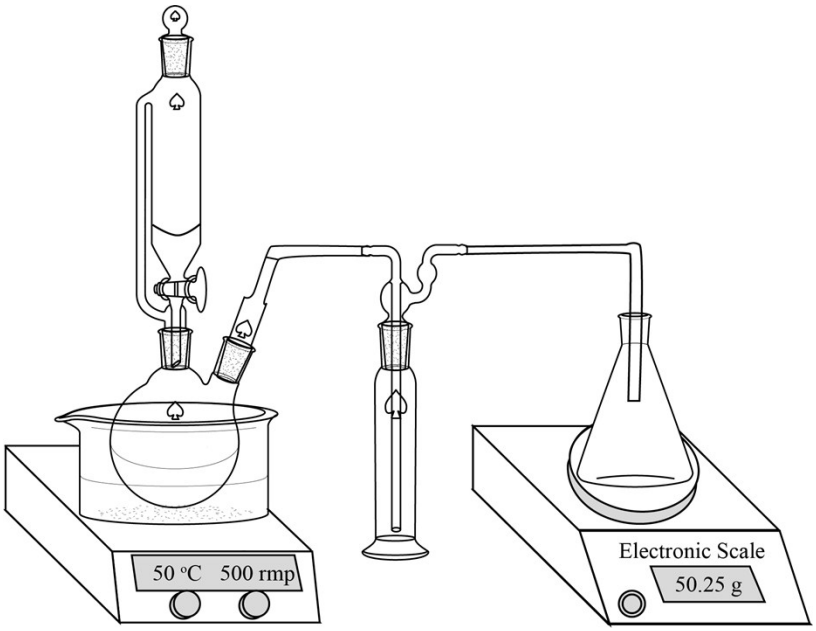

Figure S4 Schematic of hydrogen production from FA decomposition measurement system.

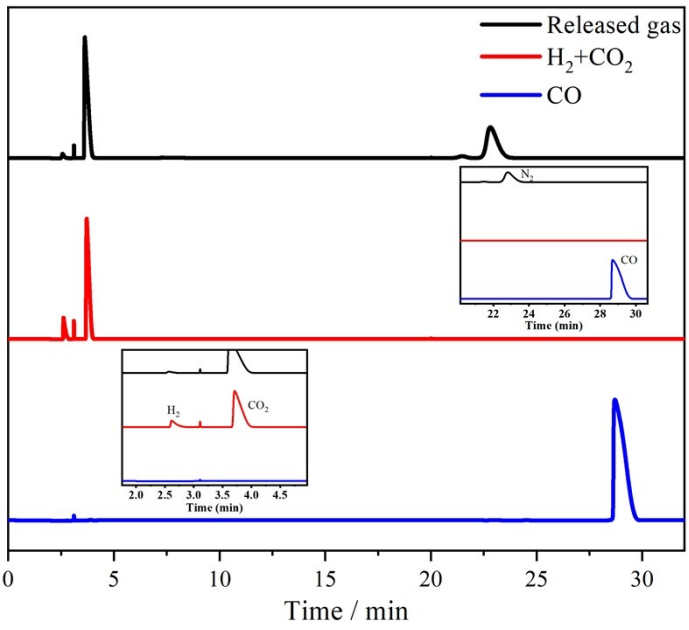

Figure S5 Gas chromatograms of air, CO_2 as reference gases and the released gas from the decomposition of FA in the presence of AP-SiO_2@PDA-NGO@Pd without any addictive at 323 K (FA: 1.06 M, 5 mL; n_{Pd}/n_{FA}=0.0028).

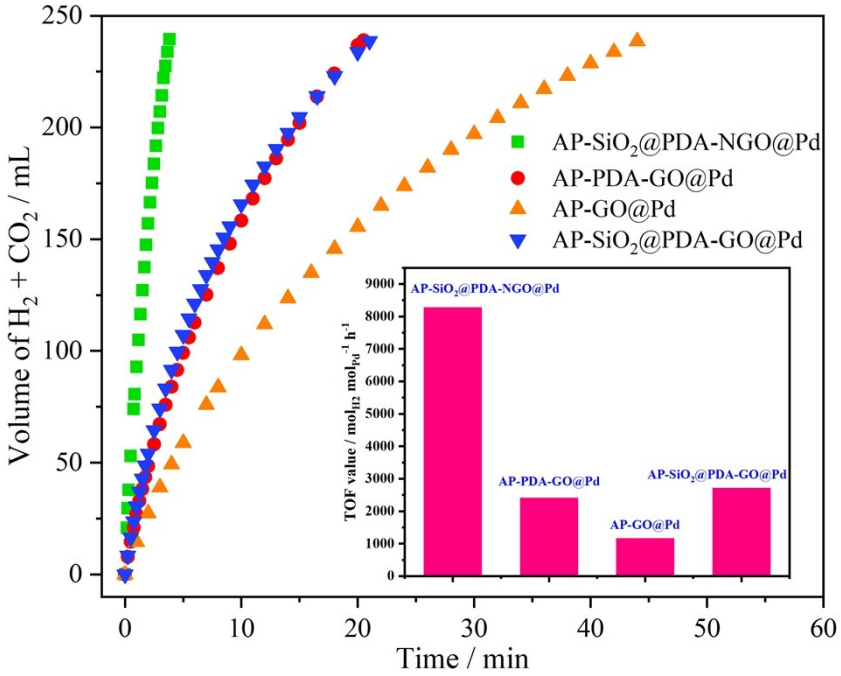

Figure S6 The time dependent hydrogen evolution curves for the dehydrogenation of formic acid catalyzed by AP-PDA-GO@Pd, AP-GO@Pd and AP-SiO_2@PDA-GO@Pd comparing with AP-SiO_2@PDA-NGO@Pd (the inset shows the corresponding TOF values; conditions: 5 mL 1.06 M FA, n_{Pd}/n_{FA}=0.0028, 323 K).

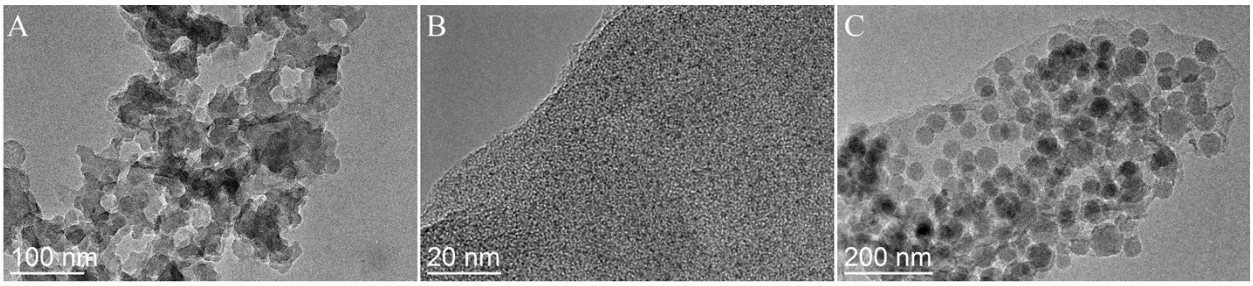

Figure S7 TEM image of NGO (A), AP-PDA-GO@Pd (B) and AP-SiO_2@PDA-GO@Pd.

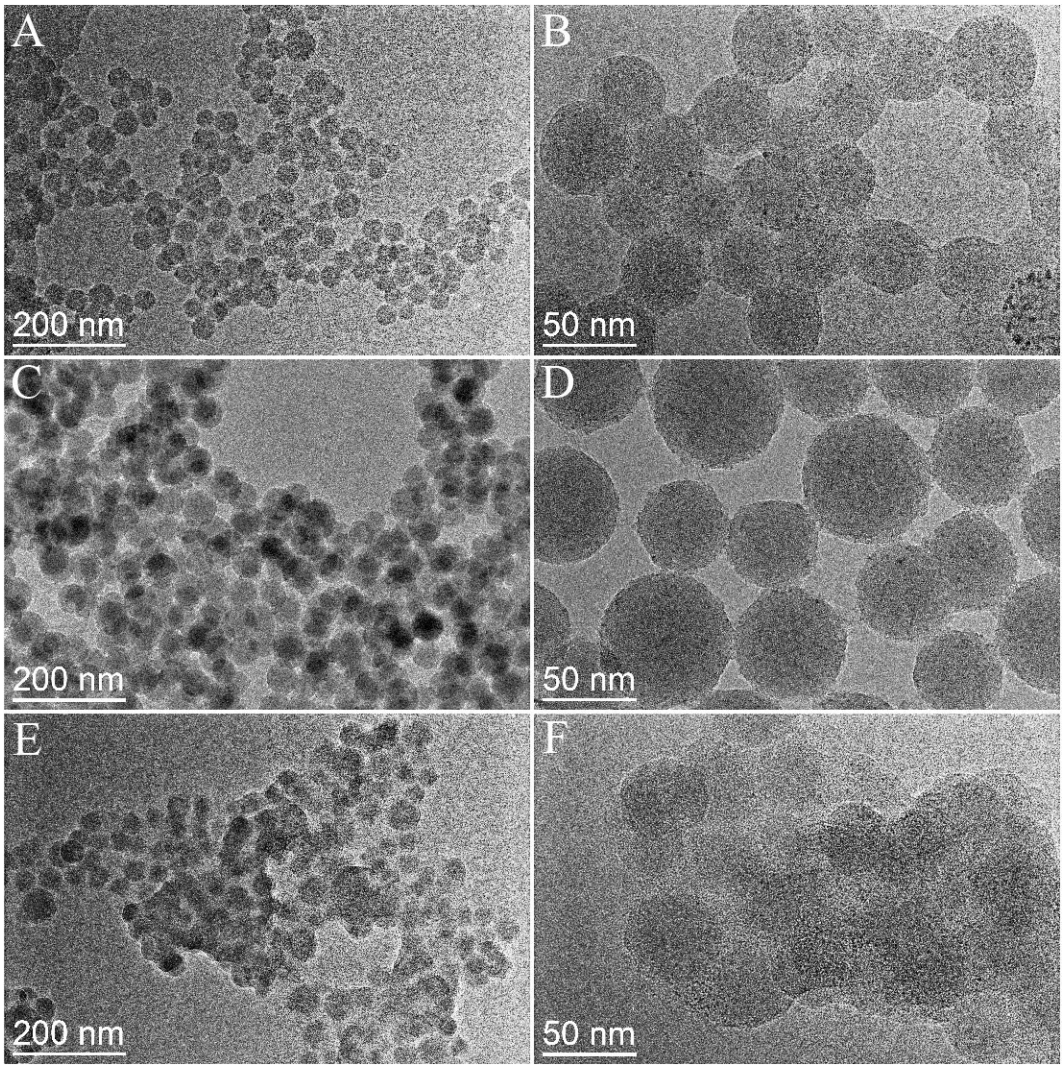

Figure S8 TEM images of catalysts with different NGO loadings (A and B: 0.5 wt%; C and D: 2 wt%; E and F: 5 wt%).

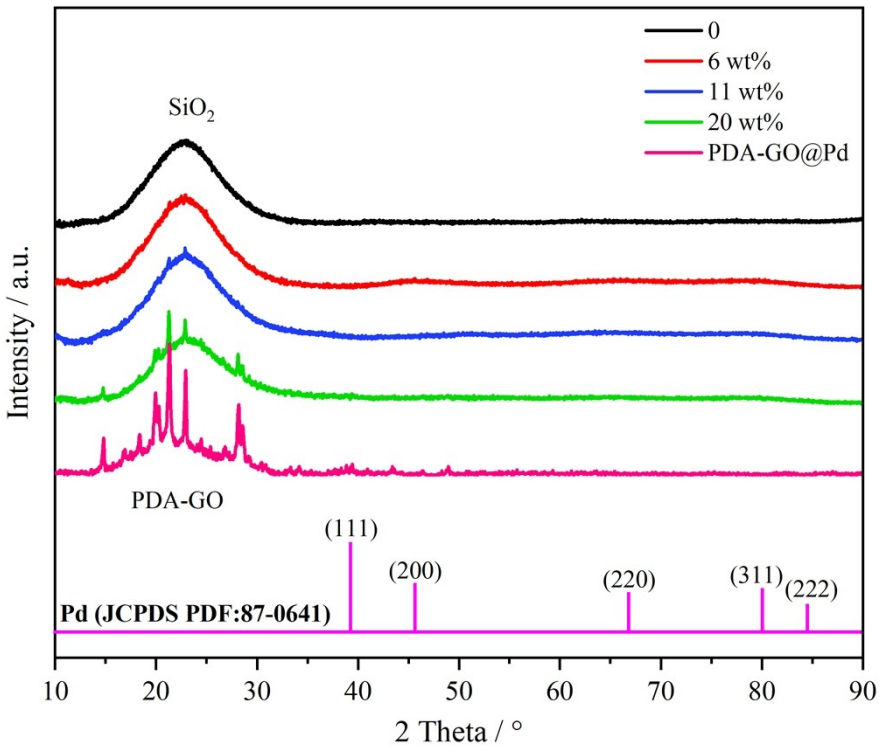

Figure S9 XRD patterns of PDA-GO@Pd and AP-SiO_2@PDA-NGO@Pd with different amounts of APTES.

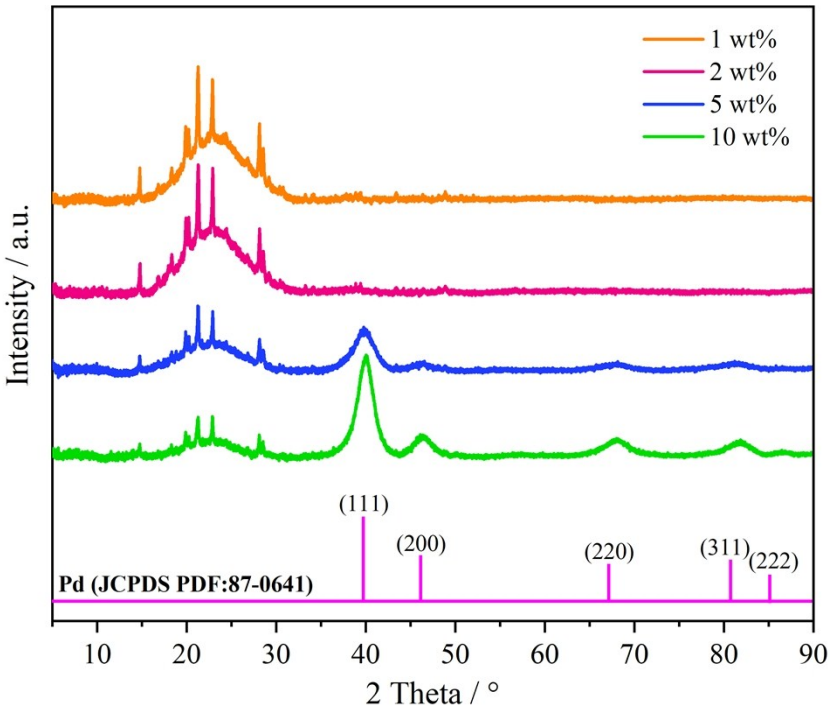

Figure S10 XRD patterns of AP-SiO_2@PDA-NGO@Pd with different loading amounts of Pd.

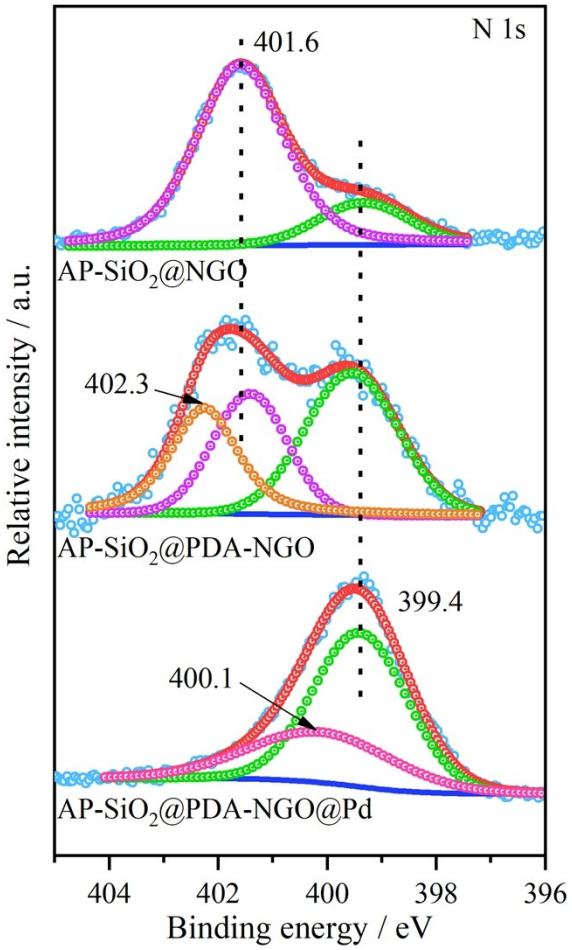

Figure S11 High-resolution X-ray photoelectron spectroscopy (XPS) spectra of N 1s in specimens AP-SiO_2@NGO, AP-SiO_2@PDA-NGO and AP-SiO_2@PDA-NGO@Pd.

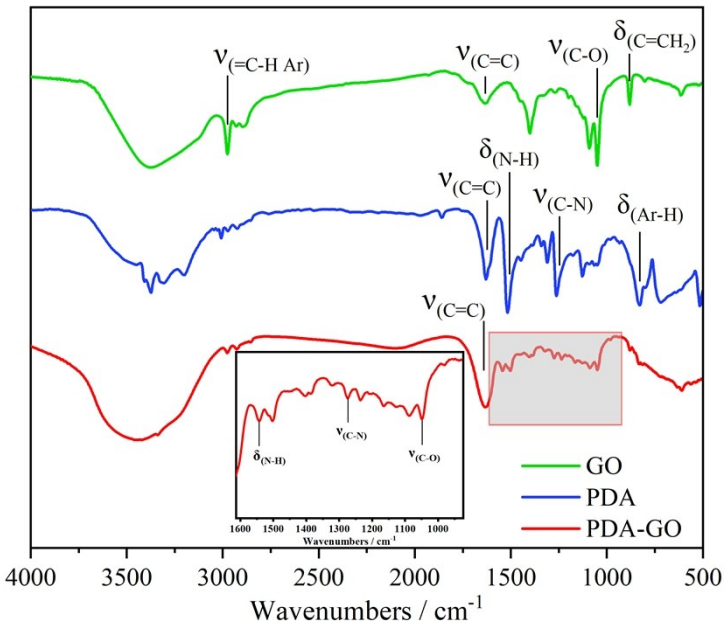

Figure S12 IR spectra of GO, PDA and PDA-GO.

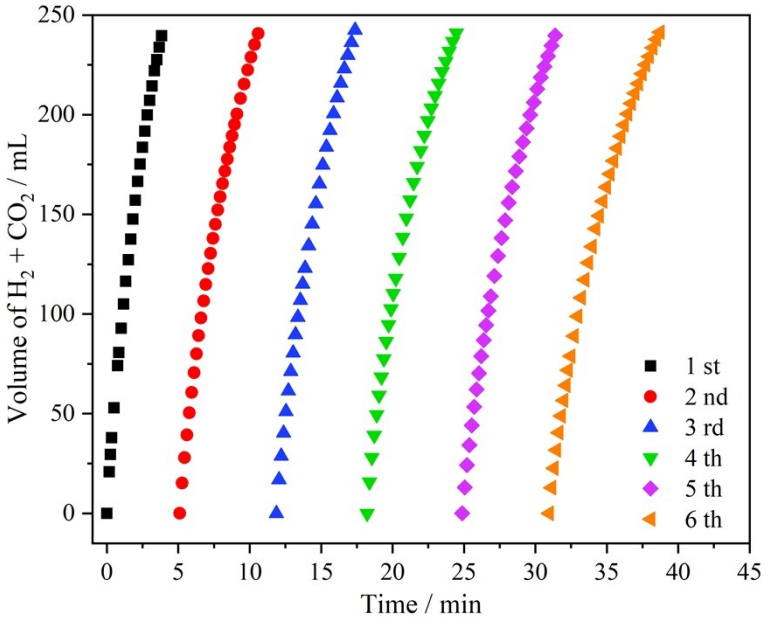

Figure S13 Durability test of AP-SiO_2@PDA-NGO@Pd in six runs for catalytic dehydrogenation of formic acid at 323 K (FA: 1.06 M, 5 mL; n_{Pd}/n_{FA}=0.0028).

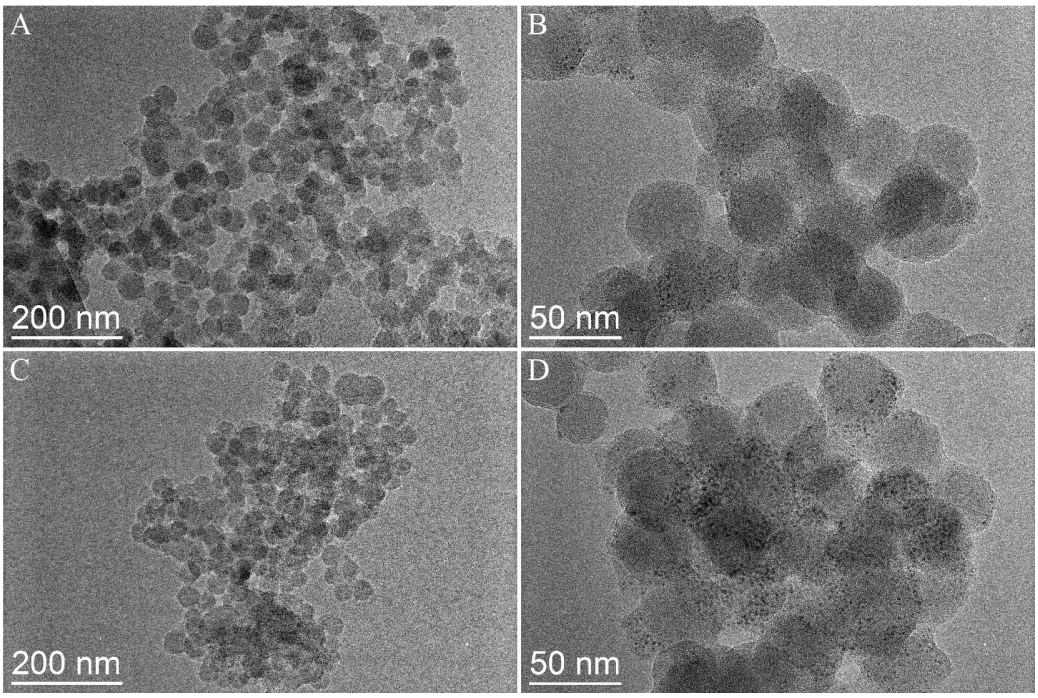

Figure S14 TEM images of AP-SiO_2@PDA-NGO@Pd before (A, B) and after (C, D) 6 cycles for catalytic decomposition of formic acid.

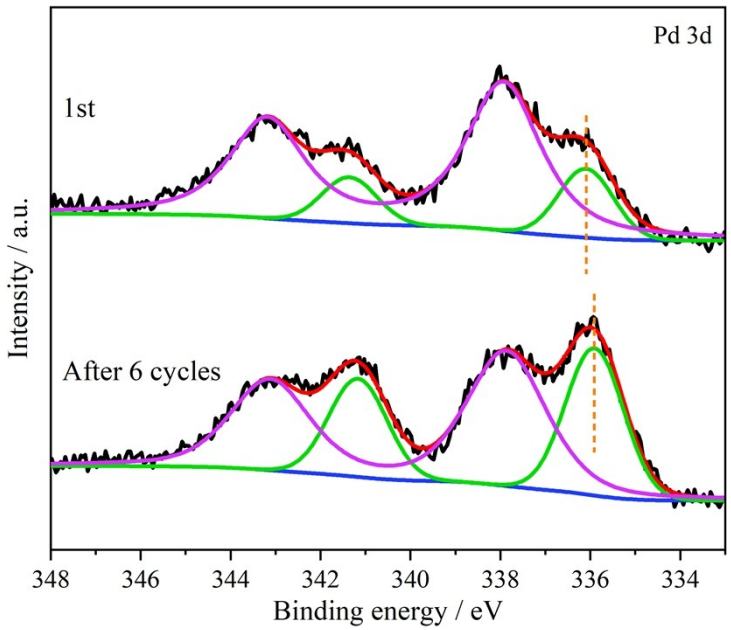

Figure S15 High-resolution X-ray photoelectron spectroscopy (XPS) spectra of Pd 3d in AP-SiO_2@PDA-NGO@Pd before and after 6 cycles for catalytic decomposition of formic acid.

Table S1. Catalytic activity comparison with recently reported Pd-based catalysts for dehydrogenation of formic acid.

Catalyst	Temp (°C)	Metal/FA molar ratio	SF/FA molar ratio	Initial TOF (h^{-1})	Ref
Pd/S-1-in-K	50	0.01	1	3027	[9]
Au_1Pd_2/GO	25	0.02	1	954.2	[10]
$Pd_{0.6}Ag_{0.4}$@ZrO_2/C/rGO	60	0.027	2.5	4500	[11]
$Ag_{0.1}Pd_{0.9}$/rGO	25	0.02	0.67	105.2	[12]
PdAg/amine-MSC	75	0.0016	0.11	5638	[13]
NiPd/NH_2-N-rGO	25	0.02	0	954.3	[14]
$(Co_6)Ag_{0.1}Pd_{0.9}$/RGO	50	0.02	2.5	2739	[15]
$(Co_3)_EAu_{0.6}Pd_{0.4}$/RGO	50	0.02	2.5	4840	[16]
Pd/C_m	60	0.006	1	7256	[17]
PdCoNi/TiO_2-ALD-SiO_2	25		1	207	[18]
Pd/PDA-rGO	50	0.015	1	3810	[19]
$Pd_{0.5}Au_{0.3}Mn_{0.2}$/N-SiO_2	25		0	785	[20]
AuPd-MnO_x/ZIF-8-rGO	25	0.013	0	382.1	[21]
Pd_5Ag_5NWs	25		0	312	[22]
Pd@CN900K	50	0.017	3	8000	[23]
AP-SiO_2@PDA-NGO@Pd	**65**	**0.0028**	**0**	**18625**	**This work**
AP-SiO_2@PDA-NGO@Pd	**50**	**0.0028**	**0**	**8274**	**This work**
AP-SiO_2@PDA-NGO@Pd	**25**	**0.0028**	**0**	**1588**	**This work**

Table S2. Content of Pd in catalysts with different supports based on ICP-AES analysis.

Sample	Content of Pd (mg/L)	Pd content in catalysts (%)		Loading percentage (%)
		Practical	Theoretical	
[a]PDA-GO@Pd	7.913	4.0	10	40
[b]AP-SiO_2@PDA-NGO@Pd	3.831	1.9	2	95

[a)] For the ICP analysis, 10 mg of product was dissolved with the mixture of 3 mL $HClO_4$ and 3 mL concentrated nitric acid, and then heated to 160 °C for totally dissolved. Finally, the solution was diluted to 50 mL in a volumetric flask.

[b)] 10 mg of product was dissolved with 1 mL of HF and 1 mL of aqua regia, and then diluted to 50 mL in a volumetric flask. Practical Pd content = content of Pd based on ICP-AES × volume of solution (0.005 L) × 100% / (amount of catalyst (0.01 g)). Theoretical Pd content = amount of Pd^{2+} precursor added / (total amount of catalyst). Loading percentage of Pd = practical Pd content in catalyst / (theoretical Pd content in it).

Table S3. Calculated vibrational frequencies (cm^{-1}) of intermediates adsorbed on Pd(111) and PDA-NGO@Pd_8.

System	Intermediates	Vibrational frequencies (cm^{-1})
Pd(111)	HC*OO*H	374.10, 345.46, 201.82, 168.16, 160.37, 142.45, 122.53, 88.11, 79.63, 28.13, 24.31, 20.47, 10.14
	HC*O*O +*H	365.33, 184.90, 163.21, 159.98, 139.99, 123.17, 120.21, 89.73, 77.21, 37.83, 37.12, 30.38, 18.14, 6.93
	HCO*O + *H	305.94, 208.63, 158.06, 140.52, 132.02, 117.59, 110.03, 97.76, 86.04, 36.53, 22.24 19.26, 17.39, 6.14
	2*H	125.90, 125.45, 105.61, 103.81, 102.27, 98.63
PDA-NGO@Pd_8	H*C*OOH	451.72, 371.44, 183.52, 158.81, 154.03, 126.03, 103.73, 71.78, 67.36, 43.94, 33.74, 20.04, 8.09
	HC*OO +*H	350.65, 236.61, 201.80, 178.60, 166.75, 163.85, 149.22, 121.90, 91.58, 38.77, 30.66, 22.22, 19.74, 17.01, 4.43
	*C*OO +2*H	349.93, 229.40, 153.75, 18.32, 144.85, 134.98, 124.08, 80.78, 70.24, 66.00, 34.86, 30.59, 18.26, 12.52, 11.25
	2*H	270.57, 182.63, 159.75, 149.03, 76.00, 57.03

Table S4. Zero-point energies (ZPE) and entropies (*S*) of reaction intermediates adsorbed on Pd(111), PDA-GO@Pd_8.

System	Intermediates	ZPE (eV)	*S* (eV/K)
Pd(111)	HC*OO*H	0.8828	0.000493
	HC*O*O + *H	0.7771	0.000563
	HCO*O + *H	0.7291	0.000653
	2*H	0.3308	0.000041
PDA-NGO@Pd_8	H*C*OOH	0.8971	0.000477
	HC*OO + *H	0.8969	0.000732
	*C*OO + 2*H	0.8049	0.000646
	2*H	0.4475	0.000056

Table S5. Gibbs free energy of formation (ΔG) for each elements step of FA decomposition on Pd(111) and PDA-NGO@Pd_8.

	Step	Reaction	ΔE / eV	ΔG / eV
Pd(111)	R1	HCOOH → HC*OO*H	–0.76	0.09
	R2	HC*OO*H → HC*O*O + *H	–0.07	–0.20
	R3	HC*O*O + *H → HCO*O + *H	0.64	0.57
	R4	HCO*O + *H → CO_2 + 2*H	–1.20	–1.20
	R5	2*H → H_2	1.28	0.80
PDA-NGO@Pd_8	R1	HCOOH → H*C*OOH	–1.00	–0.14
	R2	H*C*OOH → HC*OO + *H	–0.27	–0.41
	R3	HC*OO + *H → *C*OO + 2*H	0.02	0.07
	R4	*C*OO + 2*H → CO_2 + 2*H	0.28	0.24
	R5	2*H → H_2	0.90	0.34

References

1. G. Kresse; J. Furthmuller, *Phys. Rev. B* **1996,** *54* (16), 11169-11186.

2. G. Kresse; D. Joubert, *Phys. Rev. B* **1999,** *59* (3), 1758-1775.

3. J. P. Perdew; K. Burke; M. Ernzerhof, *Phys. Rev. Lett.* **1996,** *77* (18), 3865-3868.

4. S. Grimme; J. Antony; S. Ehrlich; H. Krieg, *J. Chem. Phys.* **2010,** *132* (15), 154104.

5. G. Henkelman; B. P. Uberuaga; H. Jonsson, *J. Chem. Phys.* **2000,** *113* (22), 9901-9904.

6. M. D. Segall; R. Shah; C. J. Pickard; M. C. Payne, *Phys. Rev. B* **1996,** *54* (23), 16317-16320.

7. S. J. Clark; M. D. Segall; C. J. Pickard; P. J. Hasnip; M. J. Probert; K. Refson; M. C. Payne, *Z. Kristallogr.* **2005,** *220* (5/6), 567-570.

8. J. S. Yoo; Z. J. Zhao; J. K. Norskov; F. Studt, *ACS Catal.* **2015,** *5* (11), 6579-6586.

9. N. Wang; Q. Sun; R. Bai; X. Li; G. Guo; J. Yu, *J. Am. Chem. Soc.* **2016,** *138* (24), 7484-7487.

10. P. Liu; X. Gu; H. Zhang; J. Cheng; J. Song; H. Su, *Appl. Catal., B* **2017,** *204*, 497-504.

11. F.-Z. Song; Q.-L. Zhu; X. Yang; W.-W. Zhan; P. Pachfule; N. Tsumori; Q. Xu, *Adv. Energy Mater.* **2017,** *8* (1), 1701416.

12. Y. Ping; J.-M. Yan; Z.-L. Wang; H.-L. Wang; Q. Jiang, *J. Mater. Chem. A* **2013,** *1* (39), 12188-12191.

13. S. Masuda; K. Mori; Y. Futamura; H. Yamashita, *ACS Catal.* **2018,** *8* (3), 2277-2285.

14. J. M. Yan; S. J. Li; S. S. Yi; B. R. Wulan; W. T. Zheng; Q. Jiang, *Adv. Mater.* **2018,** *30* (12), e1703038.

15. Y. Chen; Q. L. Zhu; N. Tsumori; Q. Xu, *J. Am. Chem. Soc.* **2015,** *137* (1), 106-109.

16. X. Yang; P. Pachfule; Y. Chen; N. Tsumori; Q. Xu, *Chem. Commun.* **2016,** *52* (22), 4171-4174.

17. Q. L. Zhu; N. Tsumori; Q. Xu, *J. Am. Chem. Soc.* **2015,** *137* (36), 11743-11748.

18. N. Caner; A. Bulut; M. Yurderi; I. E. Ertas; H. Kivrak; M. Kaya; M. Zahmakiran, *Appl. Catal., B* **2017,** *210*, 470-483.

19. F.-Z. Song; Q.-L. Zhu; N. Tsumori; Q. Xu, *ACS Catal.* **2015,** *5* (9), 5141-5144.

20. Y. Karatas; A. Bulut; M. Yurderi; I. E. Ertas; O. Alal; M. Gulcan; M. Celebi; H. Kivrak; M. Kaya; M. Zahmakiran, *Appl. Catal., B* **2016,** *180*, 586-595.

21. J.-M. Yan; Z.-L. Wang; L. Gu; S.-J. Li; H.-L. Wang; W.-T. Zheng; Q. Jiang, *Adv. Energy Mater.* **2015,** *5* (10), 1500107.

22. H. Liu; B. Huang; J. Zhou; K. Wang; Y. Yu; W. Yang; S. Guo, *J. Mater. Chem. A* **2018,** *6* (5), 1979-1984.

23. H. Zhong; M. Iguchi; M. Chatterjee; T. Ishizaka; M. Kitta; Q. Xu; H. Kawanami, *ACS Catal.* **2018,** *8* (6), 5355-5362.